INTERFACE

royalsocietypublishing.org/journal/rsif

Research

Cite this article: Weston K, Zhu HA, Taylor GK, Harvey C. 2026 Stability shifts in gliding flight: hawks morph from an unstable to stable state when navigating a gap. *J. R. Soc. Interface* **23**: 20250868.
https://doi.org/10.1098/rsif.2025.0868

Received: 21 August 2025
Accepted: 5 January 2026

Subject Category:
Life Sciences–Engineering interface

Subject Areas:
biomechanics

Keywords:
bird flight, morphing, flight stability, manoeuvre

Author for correspondence:
Christina Harvey
e-mail: harvey@ucdavis.edu

Electronic supplementary material is available online at https://doi.org/10.6084/m9.figshare.c.8286599.

THE ROYAL SOCIETY PUBLISHING

Stability shifts in gliding flight: hawks morph from an unstable to stable state when navigating a gap

Kiran Weston[1], Huanglun Adam Zhu[2], Graham Keith Taylor[1] and Christina Harvey[2]

[1]Department of Biology, University of Oxford, Oxford OX1 3SZ, UK
[2]Department of Mechanical and Aerospace Engineering, University of California Davis, Davis, CA 95616, USA

KW, 0009-0002-7090-3961; HAZ, 0009-0003-8318-3657; GKT, 0000-0001-8289-755X; CH, 0000-0002-2830-0844

Birds control their flight by morphing their wing and tail configurations as they shift between steady glides and agile manoeuvres. Cadaveric studies have shown that birds have the capacity to adopt both stable and unstable configurations, but it remains unknown how birds exploit this ability in flight. Here, we fill this gap by studying the progression of wing and tail configurations of a free-gliding Harris's hawk (*Parabuteo unicinctus*) during a wing-tucking manoeuvre. Wind tunnel experiments on three-dimensional-printed models revealed that tucked configurations were statically stable, while spread configurations displayed a nonlinear relationship between pitching moment and lift. This nonlinearity allows configurations to be either stable or unstable depending on the lift state, affording a previously under-explored source of flight performance flexibility. Furthermore, we found that the hawk transitioned from an unstable, spread configuration to a stable, tucked configuration as it traversed the gap, shifting the effective static margin from −25% to 19% of the reference chord. This notable stability shift suggests that adaptive flight control allows transition between flight modes and offers insight into flight conditions where shifting stability states may be relevant. This outcome will advance novel bio-inspired, fixed-wing uncrewed aerial vehicle designs capable of rapid transitions.

1. Introduction

Birds possess an inherently adaptable flight morphology that allows them to respond to changing conditions and objectives. Not only can birds perform steady fixed-wing glides over long migrations [1] or transient darting manoeuvres in pursuit of prey [2], but they are also capable of shifting between these flight modes as the situation demands [3,4]. In part, this adaptability is afforded by morphing, the ability to change the shape and orientation of the wings and tail, which alters the aerodynamic performance and stability characteristics of the flyer [5–7]. This allows birds to far exceed the manoeuvrability of fixed-wing uncrewed aerial vehicles (UAVs) while flying under similar conditions [8].

Recent fixed-wing UAV designs have sought to incorporate morphing to enhance manoeuvrability or to negotiate gaps, though without careful gain scheduling or expert manual compensation this can result in a notable deterioration of the stability and control characteristics [9–13]. Therefore, with growing interest in developing UAVs that can operate flexibly and adaptably in cluttered urban environments, avian morphing flight can provide an important source of bio-inspiration for future UAV design. However, the true

extent of morphing that birds use in flight remains unquantified, limiting our understanding of when and how morphing is used to affect flight performance.

To address this, we investigated the range of morphing used in gliding flight during a simple, approximately symmetric manoeuvre and quantified its consequences for static pitch stability. Longitudinal static stability refers to the initial pitching tendency of a flyer that is disturbed from equilibrium. A flyer is said to be statically stable if its initial pitching response to a perturbation returns the bird towards a balanced equilibrium state that generates positive lift, known as a trim state [6]. Although static stability neglects the subsequent time-history of the response, assessing the static stability of different configurations nevertheless provides an informative first step towards a comprehensive understanding of avian stability because it is a necessary condition for complete stability [5]. In this study, we isolated longitudinal stability (i.e. pitch) from lateral stability (i.e. roll, yaw) to focus on pitch control, which critically affects altitude and stall [14]. Longitudinal static stability is often quantified as the rate of change of the pitching moment with a change in angle of attack; however, it is challenging to appropriately define the angle of attack across configurations of a morphologically complex, morphing bird wing. Instead, to ensure consistency and because drag contributions are low, we use another common method to define longitudinal static stability: the pitch-stability derivative, which quantifies the rate of change of the pitching moment with a change in lift [5,15].

Stability is an informative metric that describes the resistance to departing from an equilibrium state, whether due to external disturbances or voluntary movements. As such, a more stable flight configuration is also less manoeuvrable [14,16]. Unstable flight configurations instead exacerbate perturbations allowing manoeuvres to be achieved with reduced control effort. This trade-off can therefore be adjusted to suit different flight contexts and aims; compare the design of unstable fighter aircraft to that of stable commercial airliners. Both stable and unstable configurations could be effective in different avian flight contexts, either by minimizing the active energy role of muscles in maintaining a specific pitch angle in stable configurations [17] or allowing sharp manoeuvres in unstable configurations [6].

Unlike traditional aircraft, birds have the capacity to shift between stable and unstable states through morphing [16]. However, when, and even if, this shift occurs in avian flight remains unknown. This is in part because obtaining data that captures the variable geometries of birds through a biologically relevant range of motion is challenging. Morphing alters flight dynamics through coupled changes to the spanwise sweep, dihedral and twist of the wings and tail that characterize avian flight configurations [8,17]. As such, evaluating the stability envelope of an entire morphing range from *in vivo* avian flight is necessary to better understand the ecology of birds and inform the design of next-generation fixed-wing UAVs. Advances in modern motion capture methods make it possible to extract live-gliding flight configurations at high resolution to analyse and ultimately quantify the stability characteristics that birds use in gliding flight.

Here, we quantified the range of morphing and longitudinal static stability of a live free-gliding Harris's hawk (*Parabuteo unicinctus*) performing a tucking manoeuvre. We labelled a Harris's hawk individual with retroreflective markers and recorded it gliding through a gap obstacle of varied widths, from 37 to 70 cm, in a series of flight trials (total trials, n = 28) (figure 1*a*). Using motion capture tools developed by the Oxford Flight Group [18–20], we isolated five flight configurations from a flight trial at 37 cm gap size to maximize the range of *in vivo* morphing observed in flight, from a fully extended wingspan to fully tucked. These configurations were reconstructed as three-dimensional models using biologically relevant aerofoils and a symmetric body section based on the hawk's morphology [21,22]. The flight configurations were then three-dimensional printed in resin at 73% scale for aerodynamic evaluation in the University of California (UC) Davis Aeronautical Wind Tunnel. Each configuration was mounted to a six-axis load cell to measure the lift and pitching moment produced across an angle of attack range of −20° to 20° at three Reynolds numbers equivalent to those used in live flight (1, 1.25 and 1.5 × 10^5). These data allowed the calculation of the trim state and longitudinal static stability of each flight configuration to categorize whether they are stable or unstable. This work presents the first quantification of avian stability across a range of morphing configurations used by a gliding bird navigating a gap and provides evidence that a hawk can shift between stable and unstable states.

2. Material and methods

2.1. *In vivo* gliding wing configurations

We recorded the wing configurations adopted by one captive-bred Harris's hawk individual performing a tucking manoeuvre during free-gliding flight using a motion capture system. Flights were performed at the University of Oxford's flight hall (windowless hall measuring 20.2 m long by 6.1 m wide). The Harris's hawk was recorded gliding in one direction between two perches placed 14 m apart. We used positive reinforcement to motivate the bird to perform the flights by presenting a small food reward on each perch. An intervening gap obstacle formed by two soft poles was placed 1.5 m ahead of the target perch to elicit a wing tuck manoeuvre in gliding flight, a distance informed by previous work [18]. The gap width was varied between 30, 37, 50 and 70 cm and multiple flights were performed for each width (n = 15, 25, 15 and 10, respectively). Fifty-six retroreflective markers were attached to feathers on the wings and tail to allow reconstruction of a flight configuration outline in software (figure 1*a*) [18]. The marker accuracy was sub-millimetre across all recorded flights with the residual error mean of 0.665 mm and standard deviation of 0.333 mm aligning with previous experiments [20]. Data were post-processed to remove flights where the bird contacted the pole or did not complete the full behaviour, as well as flights corrupted by erroneous marker tracking data. All 30 cm flights did not satisfy these requirements and thus were removed from this study. Therefore, we restricted the analysis to n = 28 trials (37 cm, n = 10; 50 cm, n = 11; and 70 cm, n = 7).

The flights were recorded with 20 high-speed motion capture cameras (VICON Vantage 16) with a resolution of 4096 × 4096 px at 120 Hz in VICON Nexus 2.14 software. The three-dimensional marker coordinates for each frame were reconstructed

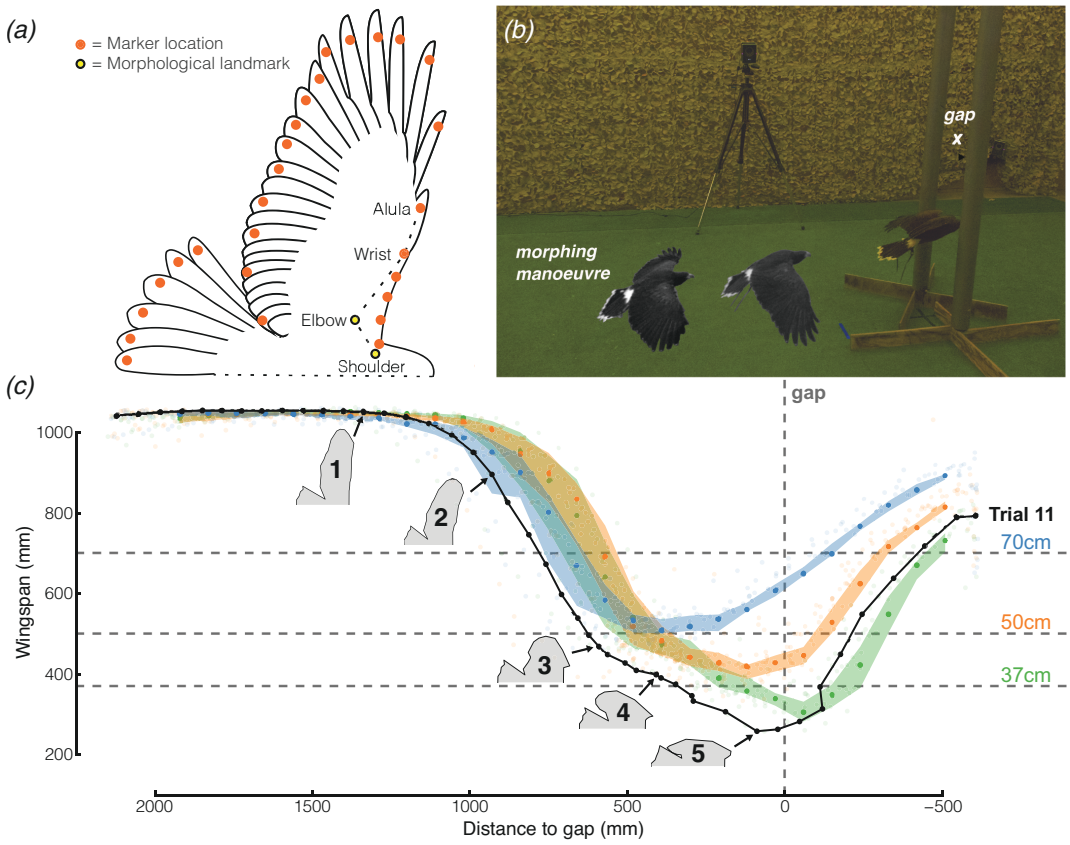

Figure 1. A Harris's hawk over-tucks for larger gap challenges. A Harris's hawk (*a*) was fitted with retroreflective markers at relevant physiological locations to provide a wing and tail outline. The subject was recorded flying between two perches placed 14 m apart down the length of the Oxford Flight lab flight hall (*b*), with an intervening gap obstacle of varying size (37, 50 or 70 cm) presented during the gliding phase to elicit a morphing response. Using motion capture software, the extent of morphing was examined over the course of multiple trial flights (37 cm, $n = 10$; 50 cm, $n = 11$; and 70 cm, $n = 7$) from three-dimensional marker motion (*c*). An interquartile range for each gap size challenge is shown to indicate a typical morphing range across the trials for each of these categories (37 cm, green; 50 cm, orange; and 70 cm, blue). Five frames were selected from flight trial 11 (black line, 37 cm gap) to obtain flight configurations (planforms in grey) representing the maximum range of morphing used in flight.

using a Python script to represent the distinct flight configurations adopted at each frame. We isolated five flight configurations for three-dimensional modelling from flight trial 11 (gap width of 37 cm), where configuration 1 is the most extended configuration and configuration 5 is the most tucked. This trial was selected as it captured a full range of morphing from maximum to minimum wingspan with minimal marker occlusion (black line and configurations, figure 1*b*). The wingspan progression observed in this trial lies outside the interquartile range of all trials at gap size 37 cm such that the configurations isolated involve a greater degree of tucking than in other flight trials captured, allowing us to investigate the greatest range of flight morphologies used by the hawk.

2.2. Model design and manufacture

Physical models of the five morphing flight configurations were generated in SolidWorks 2022 using the three-dimensional motion capture data obtained from the 44 peripheral markers placed on the hawk's wing and 12 peripheral markers placed on the hawk's tail. This work focused on an approximately symmetric manoeuvre, so we selected three-dimensional marker coordinates from only one wing (22 markers) and one half of the tail (six markers). The three-dimensional marker coordinates of one wing were joined with straight lines to define an outline, with the shoulder marker to 12th secondary feather (S12) marker representing the wing root chord. For the two most tucked configurations, S9 was used rather than S12, as the S12 marker became occluded when the wing was tucked. The three-dimensional marker coordinates of the half tail were also joined to obtain an outline, with one additional point added to represent the 'tail base' where the tail attaches to the body section. With this modelling approach, we estimated the discretized form of the twist, chord, sweep and dihedral distributions along the span of the wing and tail at each of the considered five frames based on the tracked peripheral markers. Of note, these discretized configurations are obtained from the *in vivo* flights ensuring that the configurations correspond to aerodynamically loaded configurations.

We next lofted along the span to create the three-dimensional wing shape. This required that we select three aerofoils to distribute along the wingspan to approximate the biologically relevant aerofoils. For the interior sections, we used two aerofoils obtained from a high-resolution scan of a steppe eagle (*Aquila nipalensis*) wing in flight (at 35% span and 84% span) [21], which is assumed to be appropriate as it is another raptor that is closely related to the Harris's hawk. For the most distal wing sections, we used a NACA 3603 aerofoil to approximate the distal feathers similar to a previous study [22]. The aerofoils assigned to

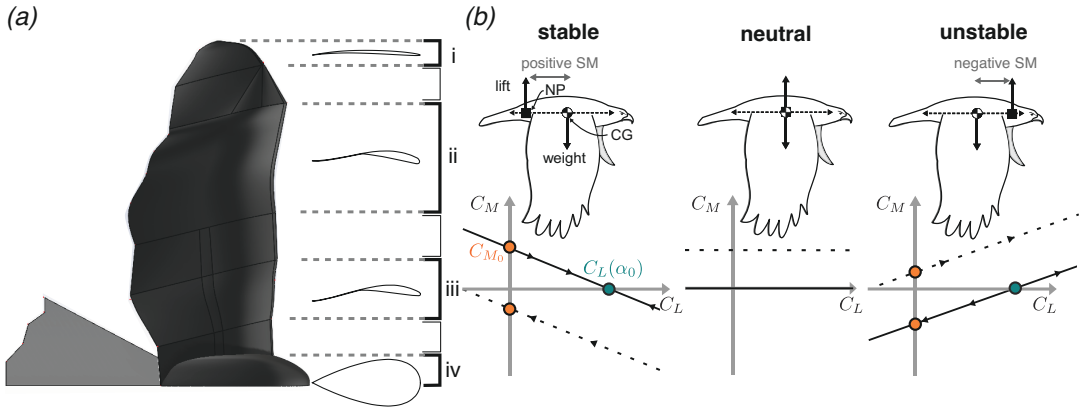

Figure 2. Three-dimensional printing of select configurations allowed the experimental evaluation of stability characteristics. (*a*) Three-dimensional models of five flight configurations across the morphing range were constructed from three-dimensional marker coordinates supplemented with biologically relevant aerofoil shapes along the span [21,22]. The aerofoils, in order from wing tip to root, are: (i) NACA 3603; (ii) 35% span from a steppe eagle [21]; (iii) 84% span from a steppe eagle [21]; and (iv) NACA0043. Half-span models of each configuration's wing, body, and tail were constructed at 73% scale for evaluation in the UC Davis Aeronautical Wind Tunnel. (*b*) The longitudinal static stability of each flight configuration was assessed through calculation of the pitch-stability derivative. Under certain assumptions (refer to the electronic supplementary material, methods for details), this value can be used to calculate the static margin, a measure of distance between the position of the centre of gravity (CG) and neutral point (NP). The static margin is inversely proportional to the rate of change of the coefficient of pitching moment (C_M) against the coefficient of lift (C_L), measured across the linear angle of attack range before stall. The static stability of each flight configuration can therefore be characterized as neutral, stable or unstable, as well as whether it is possible (solid lines) or not (dashed lines) to achieve trim at useful lift (demarcated by the green point).

each segment were based on the locations of the skeletal joints (figure 2*a*). All aerofoils were linearly blended to create a smooth wing surface, with the minimum thickness at the trailing edge increased to 0.8 mm to facilitate three-dimensional printing. The tail was modelled as a flat plane generated by performing a principal component analysis (PCA) on only the tail and tail base markers. This approach captures the dominant tail shape, and the flat-plate approximation provides a first-order estimate of the aerodynamic characteristics observed in the wind tunnel experiment.

Wing and tail sections informed by *in vivo* data were attached to a standardized half-body formed from a NACA 0043 aerofoil based on Harris's hawk body measurements (maximum length = 23 cm, maximum depth = 10.5 cm, maximum width = 10.5 cm) [22]. The body and wing sections were connected with 0° incidence angle on the wing root chord by lofting the inner edge of the wing aerofoil into a parallel aerofoil placed at the trailing edge of the body. This modelling assumption captures feather cover at the trailing edge of the wing while minimizing interference drag between the wing and body. Finally, a horizontal rectangular slot was added for tail attachment. The final models were compared in software against the original marker three-dimensional locations as validation.

We three-dimensional printed the body-wing models at 73% scale in rigid plastic (xABS-3843) using a NEXA3D NXE400 Pro resin printer and lightly sanded to smooth. The tail models were laser-cut from 0.1 inch flat acrylic at 73% scale. Each tail was bent at the junction between the tail and the rectangular attachment slot to achieve the *in vivo* tail deflection angles used by each configuration. Tails were fixed in place using super glue to form a rigid flight configuration model that did not deform under aerodynamic loading.

Note that, due to their manner of construction, the evaluation of these models neglects effects of porosity, roughness and flexibility and instead isolates the effects of morphing on longitudinal static stability. While we may expect flexibility to change in flight, these three-dimensional models reproduce an instantaneous, discretized wing shape used in flight that captures the nonlinear, coupled changes to the spanwise sweep, dihedral and twist of the wings. This complex morphology is likely to be an important contributor to stability control [9,23]. Tail effectors are also captured through the tail's span, surface area and longitudinal dihedral [24].

2.3. Statistical analysis

We fit linear models to the pre-stall wind tunnel data with the coefficient of pitching moment as the response variable and an explanatory term consisting of either first order (linear) or second order (quadratic) coefficient of lift. We report two-tailed *p*-values with a significance level of 0.05, and the coefficient of determination (R^2) for the linear model fit. When comparing between linear and quadratic representations, we computed and reported the difference between the Akaike information criterion (AIC) for each model as (δAIC), where a lower number indicates a better model fit.

2.4. Wind tunnel study

The three-dimensional-printed models were individually mounted in the UC Davis Aeronautical Wind Tunnel perpendicular to the horizontal plane. A 0.25 inch acrylic splitter plate was used to form a reflection plane leaving a 0.25 inch gap between the model and plate [25]. The models were mounted to the bottom of the wind tunnel on a six-axis load cell (ATI Mini40) that sampled at 4 kHz for 10 s. Using a custom Python script, we performed a manual angle of attack sweep for all five models

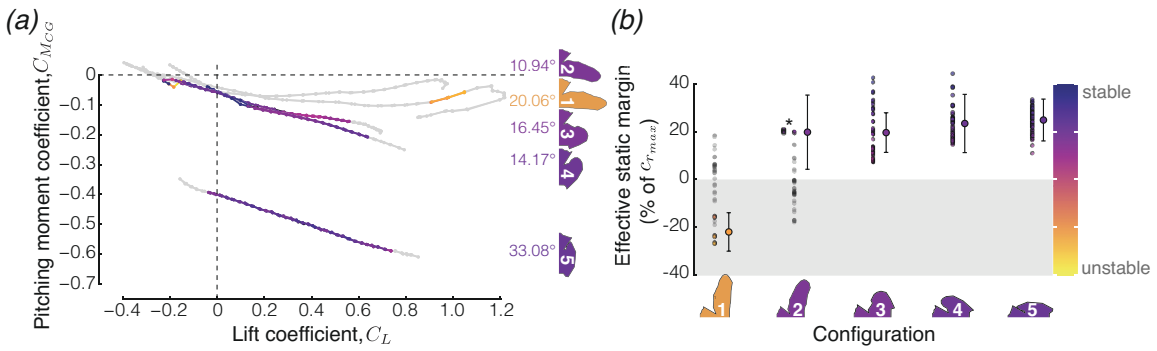

Figure 3. The hawk shifts from an unstable to stable configuration across the *in vivo* morphing range. (*a*) The coefficient of lift and pitching moment were measured across angles of attack from −20° to 20° for each configuration. This full range is shown by the complete trace, and coloured regions indicate either: the linear lift region pre-stall for configurations 3–5 or the approximate *in vivo* lift state for configurations 1–2 (see text for details). These relevant regions are coloured by the effective static margin to visualize the configuration's stability, from unstable (yellow) to stable (purple). At low lift values, all configurations showed a stable response characterized by a negative slope. At high lift values, the more extended configurations (1 and 2) shifted towards an unstable response, demonstrated by change in the slope. The large shift in the zero-lift pitching moment is in part associated with the configuration's tail deflection angle (shown on the right-hand side). (*b*) The effective static margin across the complete angle of attack sweep is indicated by a set of points to the left-hand side of each configuration with the same colour scheme as panel *a*. This captures the shift between stable and unstable states for configurations 1 and 2. The right-hand point shows the mean effective static margin of each configuration across only relevant *in vivo* flight conditions (coloured points). Error bars represent the mean within-condition standard deviations for each measurement.

from 0° to 20°, 20° to −20° and −20° to 0° with increments of 1°. The force and moment data obtained from the experiment were analysed to extract the coefficient of lift and pitching moment about the approximate centre of gravity (CG) (figure 3*a*). Each model was evaluated at three Reynolds numbers (*Re*) ranging from 1.0 to 1.5 × 10^5 with increments of 2.5 × 10^4. This range was selected to reflect the flight speeds used by the Harris's hawk individual during the flight tests. The *Re* during experiments was consistent within ± 1000. The non-dimensionalized results were not affected in this range of *Re* as demonstrated in electronic supplementary material, figure S1. The results presented in the paper are at *Re* = 1.25 × 10^5.

2.5. Centre of gravity sensitivity analysis

A critical assumption in the interpretation of our results is that the CG location of our model agrees with the actual CG of the Harris's hawk in flight. This assumption is based on previous work that quantified the uncertainty of CG location during morphing [16] and from inferences based on a closely related species. Therefore, we performed a sensitivity study by adjusting the CG between 20% of the body chord both fore and aft of the original estimated location. This study was informed by the maximum uncertainty ranges found between individuals in Harvey *et al.* [16]. Note that the variation of the CG associated with wing morphing within an individual was found to be minimal and much less than shifts associated with inter-individual differences. We found that even accounting for this large CG shift, the most spread configuration remained unstable and the most tucked configuration remained stable within our recording error. This analysis provides confidence in our result that the Harris's hawk was shifting between stable and unstable states.

One difference under these assumptions is that balanced states would be achieved at high lift conditions for configuration 4 (unstable equilibria with positive lift generation, when CG shifted at least 10% aft) or low lift conditions for configurations 1 and 2 (stable equilibria with negative lift generation, when the CG is shifted at least 5% forwards). Accounting for CG uncertainty, the observed configurations still suggest the use of active control in flight, but it remains possible that balanced flight is not entirely absent from this captured manoeuvre. This analysis highlights the sensitivity to CG position and that further study is necessary to explore the use of equilibrium states in bird flight.

3. Results and discussion

3.1. Manoeuvre behavioural insight

First, we flew a trained hawk with retroreflective markers placed on its wing and tail periphery through varied gap widths (37, 50 and 70 cm) to investigate the extent of morphing used in response to this stimulus (figure 1*a*,*b*). Wing closure as a function of distance to the obstacle was found to be largely independent of gap size at the beginning of the tucking motion, leading to the bird tucking its wings in further than required to pass the gap in the 70 cm condition (blue trace in figure 1*c*). At approximately 50 cm away from the obstacle, the rest of the tucking motion diverges markedly depending on gap size, with the bird either continuing to tuck (37 cm condition, green trace in figure 1*c*) or beginning extension of its wings (70 cm condition, figure 1*c*, blue trace). Of note, while passing through the gap, the most tucked configuration was not guaranteed to occur. The over-tucking behaviour noted for the 70 cm condition may allow the bird to account for gap size uncertainty on obstacle approach; if the gap size of an obstacle were to suddenly decrease, this behaviour would allow the bird to continue tucking

and navigate the obstacle unaffected. A future investigation into the behavioural significance of this wing tuck progression may provide additional insight into the specific use of the configurations and possible control-based advantages.

Next, to study the stability of the wing configurations used during the manoeuvre, a flight trial from the minimum gap size condition (37 cm, black trace in figure 1*c*) was selected for three-dimensional modelling. This decision allowed us to characterize stability across the greatest tucking extent demonstrated by the individual, thus presenting the largest range of biologically relevant morphing configurations with continually decreasing wingspan. The following results and conclusions focus on five flight configurations isolated from this flight trial, where configuration 1 is the most extended and configuration 5 is the most tucked (figure 1*c*).

3.2. Longitudinal stability and balance

Each of the five configurations was fabricated as half-models to be tested in the UC Davis Aeronautical Wind Tunnel (figure 2*a*, see methods for details). From these experiments, we measured and calculated the coefficient of lift (C_L) and the coefficient of pitching moment ($C_{M,CG}$), resolved about the bird's estimated CG (x_{CG}). The coefficient of lift and pitching moment were non-dimensionalized with reference to the upper wetted surface area of each individual flight configuration and the maximum root chord length ($c_{r_{max}}$) across all configurations to permit comparisons to previous work (electronic supplementary material, table S1). The CG location for the Harris's hawk was estimated to be $0.672c_{r_{max}}$ based on previous measurements on a similarly sized and closely related species, the Cooper's hawk (*Accipiter cooperii*), and assumed to remain constant across morphing [16]. The sensitivity of our results to this assumption was evaluated (refer to §2 and electronic supplementary material, figure S2).

To quantify the static pitch stability of each configuration, we used the pitch-stability derivative ($dC_{M,CG}/dC_L$), visualized as the slope between $C_{M,CG}$ and C_L for each configuration (figure 2*b*) [5,16,22]. We limited our analysis of the pitch-stability derivative to the pre-stall angle of attack range for each tested configuration (electronic supplementary material, figure S1). Based on the pitch-stability derivative, we can calculate another common metric: the static margin. The static margin is the relative distance between the CG (x_{CG}) and the neutral point (x_{NP}), the location where the pitching moment of the configuration is independent of the angle of attack [26]. For configurations undergoing small angles of attack and that have minimal contributions of axial forces, the negative pitch-stability derivative defines the static margin as a proportion of $c_{r_{max}}$ [22]. Due to the large dorsoventral offset in our configurations, in this work we do not directly translate the pitch-stability derivative to the static margin (see electronic supplementary material, methods for details and validation). Instead, we convert to an 'effective static margin' as

$$\frac{-\delta C_{M,CG}}{\delta C_L} = \text{effective static margin (\%)}$$

Stable configurations will have a positive effective static margin, while unstable configurations will have a negative effective static margin. Although this is not the true geometric static margin, it allows results to be compared across different aircraft configurations.

We found that all five flight configurations were stable at low lift conditions, demonstrated by a negative pitch-stability derivative. However, note that these low lift conditions do not necessarily provide sufficient weight support. For the most tucked flight configurations (4 and 5 in figure 3*a*), the pitch-stability derivative relationship across the full lift range was well modelled by a linear regression (configuration 4, $p < 0.001$, $R^2 = 0.9891$; configuration 5, $p < 0.001$, $R^2 = 0.9991$). These configurations exhibited consistent stable responses across all tested lift values. However, at high lift conditions, the more spread configurations (1, 2 and 3 in figure 3*a*) showed an outsized effect of changing lift on pitching moment. In fact, flight configurations 1 and 2 shifted to a positive pitch-stability derivative, indicating that the pitch stability becomes unstable at high lift conditions. The slope of configuration 3 also becomes less negative but maintains a stable response at high lift.

We found that the pitch-stability derivatives of these more spread configurations were poorly modelled by a first-order (linear) relationship (configuration 1, $p = 0.401$, $R^2 = -0.009$; configuration 2, $p = 0.005$, $R^2 = 0.190$; configuration 3, $p < 0.001$, $R^2 = 0.953$). Instead, the configurations were better represented by a second-order (quadratic) model (configuration 1, $p < 0.001$, $R^2 = 0.9680$, $\delta AIC = -70.611$; configuration 2, $p < 0.001$, $R^2 = 0.9378$, $\delta AIC = -79.623$; configuration 3, $p < 0.001$, $R^2 = 0.9988$, $\delta AIC = -114.116$).

Our results indicate that the stability of configurations used by live gliding birds cannot be assumed to have a linear relationship with lift in the pre-stall region, in contrast to fixed-wing UAVs. Traditional aerodynamic theory predicts a linear relationship between C_L and $C_{M,CG}$ in the pre-stall region because a change in lift should cause a consistent change in the pitching moment when the distance between the NP and CG remains fixed. Instead, the quadratic relationship seen in the spread configurations (1, 2 and 3) more closely resembles nonlinear relationships commonly observed in post-stall flight regions of traditional aircraft.

In this case, there are multiple possible explanations for the observed nonlinearity. One possibility is that the large variation in the twist of bird wings causes different wing sections to stall at different angles of attack, causing a shift in the location of the NP as different sections stall. Given that the overall wing does not exhibit a significant loss of lift in the investigated region (electronic supplementary material, figure S1), it is possible that the hawk's wing twist distribution may serve to functionally extend the operational angle of attack range. Another possibility is that at the low Reynolds numbers relevant to this gliding flight, laminar separation bubbles may occur and shift the NP of the wing, similar to findings on aerofoils tested at Reynolds numbers below 10^5 [27,28]. Finally, the nonlinearity may be caused by an outsized drag response associated with wing and tail interaction effects that effectively shifts the NP. This is especially possible given that the tail is located at a shorter moment arm than traditional aircraft [16]. Identifying the root cause of the nonlinear response associated with these configurations requires

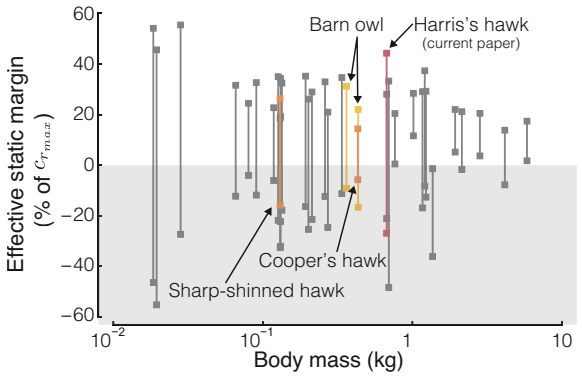

Figure 4. The maximal effective static margin range available to the hawk during the gap challenge was comparable to the previously estimated ranges for closely related avian taxa [16]. The Harris's hawk *in vivo* range, evaluated based on the maximal capabilities of the five morphing configurations (red line), was compared against the static margin range estimated from the cadaveric maximal morphing capacity of other avian taxa. Close phylogenetic relatives are highlighted. The Harris's hawk data represent the first evaluation of the pitch-stability derivative and effective static margin range in a live gliding, morphing bird, providing supporting evidence that birds shift between stable and unstable flight across a biologically relevant morphing range.

a thorough exploration of the pressure and velocity fields surrounding these wings through higher fidelity methods such as particle image velocimetry (PIV) or computational fluid dynamics (CFD). Flight in such configurations would require an active control system that could account for a state-dependent stability response of the flyer.

Next, we used the wind tunnel results to evaluate the stability of the *in vivo* flight configurations. First, we identified the flight conditions associated with each configuration. For flight configurations 1 and 2, we estimated the *in vivo* angle of attack from the forward flight speed and motion capture data, using markers placed on the right shoulder and 12th secondary feather (S12). In this calculation, we included a ±1° angle of attack error to account for potential uncertainty introduced by the omission of a constant body marker in our study. Configuration 1 and 2 were found to be gliding at an angle of attack of 4° to 6° and −3° to −5°, respectively. Note that the angle of attack used by configuration 2 is at the edge of the defined linear lift region (−3° to 13°) and is therefore marked with an asterisk (figure 3*b*). For flight configurations 3, 4 and 5, we were unable to quantify the true *in vivo* angle of attack with confidence due to marker occlusion and an inconsistent flight path. However, the pitch-stability derivative remains stable and approximately constant for these three configurations across the entire pre-stall lift range.

This analysis identified that stability shifts from a statically unstable state (configuration 1) to a stable state, with the mean normalized effective static margin ranging from −25% to 19% (visualized by the right-hand points for each configuration on figure 3*b*, where error bars indicate the mean within-condition standard deviations). Based on this analysis, we found evidence to support the conclusions of previous raptor flight studies and theoretical predictions. The fully spread wing configuration of the Harris's hawk (configuration 1) was flying in a statically unstable state, in line with findings of a barn owl in low-speed gliding flight [17]. The more tucked flight configurations adopted in response to the gap challenge were progressively more stable as tucking increased (configurations 2–5). Given the predominately linear relationship and negative pitch-stability derivative of configurations 3–5, we concluded that these configurations are statically stable over the linear lift range.

This work therefore provides the first *in vivo* evidence that a Harris's hawk can shift from unstable to stable flight via morphing through a gap obstacle. In doing so, our results question the use of a 'simple' flight control system used by birds and instead suggest that an adaptive control system would probably need to be employed to effectively maintain different stability conditions and transition between them in flight [6,16]. Furthermore, the observed range of effective static margin shift aligns with cadaver-based studies across a range of avian taxa, showing a comparable maximum effective static margin range to the Harris's hawk (−26.9% to 44.2%, see figure 4) [16].

However, of the five flight configurations evaluated, none could fly in an equilibrium state while producing positive lift, i.e. there was no static trim state. This is because there were no positive lift values that yielded a pitching moment of zero for any of the tested configurations (figure 2*b*). This finding supports previous studies that have found similar results [17,22], indicating that birds may predominately use transient configurations without a trim state and instead use active muscular control to maintain these states [29]. Note that the *in vivo* tail deflection angle (δ_t) used by the Harris's hawk in each configuration causes a greater constant nose-down pitching moment hence shifting the curves downwards (figure 3*a*). While our findings do not preclude the use of inherently stable passively controlled flight configurations in other species or different flight, it adds substantiated evidence to the use of active control in flight [6]. To explore this possibility, future studies should consider the complete dynamic stability without traditional linearized assumptions about a trim state.

Our work is only representative of the morphing configurations captured during this individual Harris's hawk's gliding, tucking manoeuvre. Other manoeuvres may not involve such large stability shifts; for example, the static margin range in the peregrine falcon, *Falco peregrinus*, calculated across three gliding configurations adopted with varying wingspan displayed a more limited range of morphing and static margin shift (−40% to 27%) [30]. Furthermore, the current study focuses on the role of overall static wing morphology in flight manoeuvres and does not capture the effects of flexibility or porosity in avian wings, as these effects are expected to be secondary to the effects of wing shape. Reducing the recorded frames to fixed three-dimensional-printed wing–tail configurations inherently assumes quasi-steady characteristics between the wing states. This assumption is justified as we designed our study to ensure that the hawk glided through the gap, avoiding the cyclic,

unsteady forces associated with its flapping flight phases. Even with this focus, future morphing models and higher-fidelity methods should explore the potential role of unsteady forces that occur between the different morphed states even within gliding.

Altogether, our results provide evidence that a hawk shifts between stable and unstable flight configurations while traversing a gap challenge. The unstable fully extended configuration may allow quick and easy control of the approach path, while the stable tucked configurations may improve the ability to reject perturbations to the flight path while navigating a tight space, such as if a feather was to contact a branch.

4. Conclusion

Here, we investigated the *in vivo* morphing used by a Harris's hawk performing a tucking manoeuvre and quantified the longitudinal static stability characteristics. We isolated five morphing configurations and characterized their stability profiles using a wind tunnel study of three-dimensional-printed models. Our results revealed that the hawk shifted between unstable and stable flight and that there was a nonlinear association between lift and pitching moment in the outstretched flight configurations. These findings suggest a unique method to control manoeuvrability that could be tuned to different flight conditions and emphasizes the need to quantify stability within the context of a desired manoeuvre to understand the application of flight morphology to control. Within the context of the elicited tucking manoeuvre, the shift between unstable and stable flight configurations throughout the manoeuvre suggests the use of a complex adaptive control system employed in avian flight. However, we found that no configurations used were able to trim, suggesting that active control inputs must constantly adjust the flight configuration during the execution of the tucking manoeuvre for the gap challenge. This work reveals previously under-explored stability characteristics of avian flight with relevance to the design of operation-flexible and adaptable fixed-wing UAVs that negotiate tight gaps. In summary, our stability characterization of a Harris's hawk tucking manoeuvre points towards the need to integrate across studies of aerodynamics, behaviour, morphology and neural control to more wholly understand the control systems of birds [20,21].

Ethics. This work was approved by the Animal Welfare and Ethical Review Board of the Department of Zoology, University of Oxford, in accordance with university policy on the use of protected animals for scientific research, permit no. APA/1/5/ZOO/NASPA, and was considered not to pose any significant risk of causing pain, suffering, damage or lasting harm to the animals.

Data accessibility. All data and code used and reported in this paper have been deposited in the public repository [31]. All other data are included in the manuscript and/or electronic supplementary material, appendix.

Supplementary material is available online [32].

Declaration of AI use. AI-assisted tools were used for spelling and grammar checks and for preliminary code set-up. All writing, analysis, and code were created and verified by the authors.

Authors' contributions. K.W.: conceptualization, data curation, formal analysis, investigation, methodology, validation, visualization, writing—original draft, writing—review and editing; H.A.Z.: investigation, methodology, validation, writing—review and editing; G.K.T.: conceptualization, funding acquisition, methodology, project administration, resources, supervision, writing—review and editing; C.H.: conceptualization, funding acquisition, investigation, methodology, project administration, resources, supervision, visualization, writing—original draft, writing—review and editing.

All authors gave final approval for publication and agreed to be held accountable for the work performed therein.

Conflict of interest declaration. We declare we have no competing interests.

Funding. This work was supported in part by the Air Force Office of Scientific Research (AFOSR) through the Bio-Inspired Sensing, Computing, and Control with International Teams (BISCCITs) Travel Grants provided to C.H. and K.W. (grant no,: FA9550-22-1-0124) and in part by the David and Lucile Packard Foundation through the Packard Fellowship in Science and Engineering provided to C.H.

Acknowledgements. Thank you to Lydia France and Marco Klein Heerenbrink for support with the analysis and interpretation of the flight data as well as to the other members of the Oxford Flight Group and the UC Davis BIRD Lab for helpful feedback and discussions. Thank you to Aaron Eppstein for his assistance in generating three-dimensional wing outlines and to Oliver Brewster for his guidance on three-dimensional printing and modelling.

References

1. Hedenström A, Åkesson S. 2016 Ecology of tern flight in relation to wind, topography and aerodynamic theory. *Phil. Trans. R. Soc. B* **371**, 20150396. (doi:10.1098/rstb.2015.0396)
2. Dakin R, Segre PS, Straw AD, Altshuler DL. 2018 Morphology, muscle capacity, skill, and maneuvering ability in hummingbirds. *Science* **359**, 653–657. (doi:10.1126/science.aao7104)
3. Cheney JA, Stevenson JPJ, Durston NE, Maeda M, Song J, Megson-Smith DA, Windsor SP, Usherwood JR, Bomphrey RJ. 2021 Raptor wing morphing with flight speed. *J. R. Soc. Interface* **18**, 20210349. (doi:10.1098/rsif.2021.0349)
4. Reynolds KV, Thomas ALR, Taylor GK. 2014 Wing tucks are a response to atmospheric turbulence in the soaring flight of the steppe eagle *Aquila nipalensis*. *J. R. Soc. Interface* **11**, 20140645. (doi:10.1098/rsif.2014.0645)
5. Harvey C, Baliga VB, Lavoie P, Altshuler DL. 2019 Wing morphing allows gulls to modulate static pitch stability during gliding. *J. R. Soc. Interface* **16**, 20180641. (doi:10.1098/rsif.2018.0641)
6. Thomas AL, Taylor GK. 2001 Animal flight dynamics I. Stability in gliding flight. *J. Theor. Biol.* **212**, 399–424. (doi:10.1006/jtbi.2001.2387)
7. Lentink D *et al*. 2007 How swifts control their glide performance with morphing wings. *Nature* **446**, 1082–1085. (doi:10.1038/nature05733)
8. Harvey C, Gamble LL, Bolander CR, Hunsaker DF, Joo JJ, Inman DJ. 2022 A review of avian-inspired morphing for UAV flight control. *Prog. Aerosp. Sci.* **132**, 100825. (doi:10.1016/j.paerosci.2022.100825)

9. Ajanic E, Feroskhan M, Mintchev S, Noca F, Floreano D. 2020 Bioinspired wing and tail morphing extends drone flight capabilities. *Sci. Robot.* **5**, eabc2897. (doi:10.1126/scirobotics.abc2897)
10. Ajanic E, Feroskhan M, Wüest V, Floreano D. 2022 Sharp turning maneuvers with avian-inspired wing and tail morphing. *Commun. Eng.* **1**, 1–9. (doi:10.1038/s44172-022-00035-2)
11. Neal D, Good M, Johnston C, Robertshaw H, Mason W, Inman D. 2004 Design and wind-tunnel analysis of a fully adaptive aircraft configuration. In *45th AIAA/ASME/ASCE/AHS/ASC Structures, Structural Dynamics & Materials Conf.*, Palm Springs, CA, p. 1727. Reston, VA, USA: American Institute of Aeronautics and Astronautics. (doi:10.2514/6.2004-1727)
12. Aloui O, Zufferey R, Stewart W, Askari M, Jeger S, Floreano D. 2025 Collision-resilient winged drones enabled by tensegrity structures. *Adv. Robot. Res.* 202500050. (doi:10.1002/adrr.202500050)
13. Henry TC, Hrynuk JT, Del Colliano A, King P. 2023 Wing strike reduction for small fixed wing uncrewed aerial vehicles. *Aerosp. Sci. Technol.* **142**, 108645. (doi:10.1016/j.ast.2023.108645)
14. Pamadi BN. 2004 *Performance, stability, dynamics, and control of airplanes*. Reston, VA: American Institute of Aeronautics and Astronautics.
15. Anderson JD Jr. 2010 *Fundamentals of aerodynamics*, 3rd edn. Columbus, OH: McGraw-Hill Education.
16. Harvey C, Baliga VB, Wong JCM, Altshuler DL, Inman DJ. 2022 Birds can transition between stable and unstable states via wing morphing. *Nature* **603**, 648–653. (doi:10.1038/s41586-022-04477-8)
17. Durston NE, Wan X, Liu JG, Windsor SP. 2019 Avian surface reconstruction in free flight with application to flight stability analysis of a barn owl and peregrine falcon. *J. Exp. Biol.* **222**, b185488. (doi:10.1242/jeb.185488)
18. KleinHeerenbrink M, France LA, Brighton CH, Taylor GK. 2022 Optimization of avian perching manoeuvres. *Nature* **607**, 91–96. (doi:10.1038/s41586-022-04861-4)
19. Brighton CH, Kempton JA, France LA, KleinHeerenbrink M, Miñano S, Taylor GK. 2023 Obstacle avoidance in aerial pursuit. *Curr. Biol.* **33**, 3192–3202.(doi:10.1016/j.cub.2023.06.047)
20. Miñano S, Golodetz S, Cavallari T, Taylor GK. 2023 Through hawks' eyes: synthetically reconstructing the visual field of a bird in flight. *Int. J. Comput. Vis.* **131**, 1497–1531. (doi:10.1007/s11263-022-01733-2)
21. Carruthers AC, Thomas ALR, Walker SM, Taylor GK. 2010 Mechanics and aerodynamics of perching manoeuvres in a large bird of prey. *Aeronaut. J.* **114**, 673–680. (doi:10.1017/s0001924000004152)
22. Harvey C, Baliga VB, Goates CD, Hunsaker DF, Inman DJ. 2021 Gull-inspired joint-driven wing morphing allows adaptive longitudinal flight control. *J. R. Soc. Interface* **18**, 20210132. (doi:10.1098/rsif.2021.0132)
23. Tran D, Lind R. 2010 Parameterizing stability derivatives and flight dynamics with wing deformation. In *AIAA Atmospheric Flight Mechanics Conf*, Toronto, Canada, p. 8227. Reston, VA: American Institute of Aeronautics and Astronautics. (doi:10.2514/6.2010-8227)
24. Thomas ALR. 1993 On the aerodynamics of birds' tails. *Phil. Trans. R. Soc. B* **340**, 361–380. (doi:10.1098/rstb.1993.0079)
25. Barlow JB, Rae WH, Pope A. 1999 *Low-speed wind tunnel testing*. Hoboken, NJ: John Wiley & Sons.
26. Anderson JD Jr. 1989 *Introduction to flight*, 3rd edn. Columbus, OH: McGraw-Hill Higher Education.
27. Ohtake T, Nakae Y, Motohashi T. 2007 Nonlinearity of the aerodynamic characteristics of NACA0012 aerofoil at low Reynolds numbers. *J. Jpn. Soc. Aeronaut. Space Sci.* **55**, 439–445. (doi:10.2322/jjsass.55.439)
28. Winslow J, Otsuka H, Govindarajan B, Chopra I. 2018 Basic understanding of airfoil characteristics at low Reynolds numbers (104–105). *J. Aircr.* **55**, 1050–1061. (doi:10.2514/1.c034415)
29. Smith JM. 1952 The importance of the nervous system in the evolution of animal flight. *Evolution* **6**, 127–129. (doi:10.1111/j.1558-5646.1952.tb02818.x)
30. Durston N. 2019 *Quantifying the flight stability of free-gliding birds of prey*. Bristol, UK: University of Bristol.
31. Weston K, Zhu HA, Taylor GK, Harvey C. 2025 Supplement to: Stability shifts in gliding flight: hawks morph from an unstable to stable state when navigating a gap. figshare (doi:10.6084/m9.figshare.c.7889849)
32. Weston K, Zhu HA, Taylor GK, Harvey C. 2026 Supplementary material from: Stability shifts in gliding flight: Hawks morph from an unstable to stable state when navigating a gap. Figshare. (doi:10.6084/m9.figshare.c.8286599)